ELSEVIER

Cycle-averaged dynamics of a periodically driven, closed-loop circulation model ☆

T. Heldt[a],*, J.L. Chang[b], J.J.S. Chen[c], G.C. Verghese[c], R.G. Mark[a]

[a]Harvard– MIT Division of Health Sciences and Technology, Massachusetts Institute of Technology, E25-505, 77 Massachusetts Avenue, Cambridge, MA 02139, USA
[b]School of Medicine, University of California, San Francisco, 513 Parnassus, S-245, Box 0454, San Francisco, CA 94143, USA
[c]Department of Electrical Engineering and Computer Science, Massachusetts Institute of Technology, 10-093, 77 Massachusetts Avenue, Cambridge, MA 02139, USA

Abstract

Time-varying elastance models have been used extensively in the past to simulate the pulsatile nature of cardiovascular waveforms. Frequently, however, one is interested in dynamics that occur over longer time scales, in which case a detailed simulation of each cardiac contraction becomes computationally burdensome. In this paper, we apply circuit-averaging techniques to a periodically driven, closed-loop, three-compartment recirculation model. The resultant cycle-averaged model is linear and time invariant, and greatly reduces the computational burden. It is also amenable to systematic order reduction methods that lead to further efficiencies. Despite its simplicity, the averaged model captures the dynamics relevant to the representation of a range of cardiovascular reflex mechanisms.
© 2004 Elsevier Ltd. All rights reserved.

Keywords: Average values; Biomedical systems; Circuits; Model reduction; Simulation; Transient analysis

1. Introduction

Over the past 30 years, computational models of cardiovascular function have become abundant in both basic research and teaching, with increasingly sophisticated models becoming available at any biological size and time scale. At the system level, time-varying ventricular elastance models have proven to be useful

representations of the right and left heart (see e.g., Sunagawa & Sagawa, 1982). When coupled to appropriate models of the peripheral systemic and pulmonary circulations, such models allow for simulation of realistic pulsatile, quasi-periodic pressure and flow waveforms. The dynamics of these models, however, are quite complex, representing cardiovascular physiology at a variety of time scales that include very fast dynamics (such as cardiac contraction) and slower dynamics (such as peripheral blood flow). Frequently one is not interested in an instantaneous value of a particular variable, or in the details of a specific waveform, but rather in the response of the variable's short-term average to perturbations in its parameters. This response typically occurs over time scales that are large compared to the dynamics of cardiac contraction.

In these cases, a cycle-averaged model, which tracks cycle-to-cycle (i.e. inter-cycle) dynamics rather than

intra-cycle dynamics, seems desirable for several reasons. First, by ignoring the fine intra-cycle structure of each waveform, one can expect to reduce computational cost significantly. Second, one can anticipate that analysis of the dynamics of interest can be simplified if the model structure is reduced sufficiently. Third, it is typically the time-averages and not instantaneous values of key state variables that are regulated through feedback control. This situation is typical of domains (from biology to power systems) in which the component processes and their interactions are fairly well mapped out. In such cases, the natural models for computation and simulation of the global behavior of the system comprise complex interconnections of models for the component processes. However, the transients produced by such complex non-linear models may look similar to the transients produced by low-order linear models.

The goal of this paper, which builds on Chang (2002), is to study a periodically driven, closed-loop, lumped-parameter recirculation model and to derive a cycle-averaged version of it by applying circuit-averaging techniques from the power electronics literature (Verghese, 1996). The process of cycle-averaging preserves the state–space description of the model. Furthermore, the resulting model structure turns out to be linear and time-invariant (LTI), which allows for further insight into and simplification of the model structure.

While the following discussion is inevitably framed from the perspective of physiological systems, we have tried to keep the domain-specific terminology to a minimum in order to make this work accessible to the broader engineering audience.

2. Pulsatile model

We implemented a simplified version of a previously published lumped-parameter, closed-loop pulsatile model (Heldt, Shim, Kamm, & Mark, 2002). While the simplified model only represents the left ventricle and the systemic circulation, it is still rich enough to capture the essential time-varying dynamics of the pulsatile model and to serve as a sufficient testbed for our development of an averaging methodology.

As shown in Fig. 1, the model is in circuit form, and consists of three segments, representing cardiac (or pumping), arterial (or high pressure), and venous (or low pressure) compartments, respectively. The pumping action of the heart is represented by a single ventricular time-varying compliance, $C(t)$ [the inverse of a time-varying elastance, $E(t)$, i.e. $C(t) = 1/E(t)$], which cycles with period T between a diastolic (or filling) value C_D of duration T_D, and a systolic (or ejection) value C_S of duration T_S, as shown in Fig. 2. We assume the duty ratio T_S/T_D to be $\frac{1}{2}$ for convenience, although other
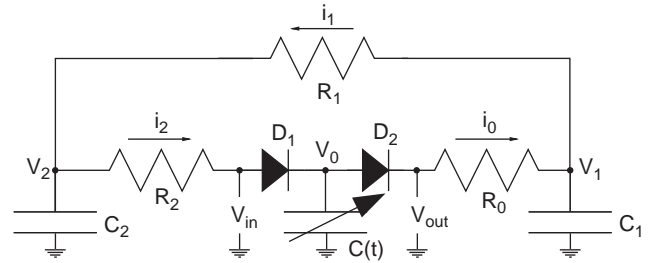

Fig. 1. Pulsatile model. $C(t)$ is a time-varying compliance; V_{in} and V_{out} are defined here for future reference (see Section 3.2); the voltages V_0, V_1, V_2 represent cardiac, arterial, and venous pressures, respectively.
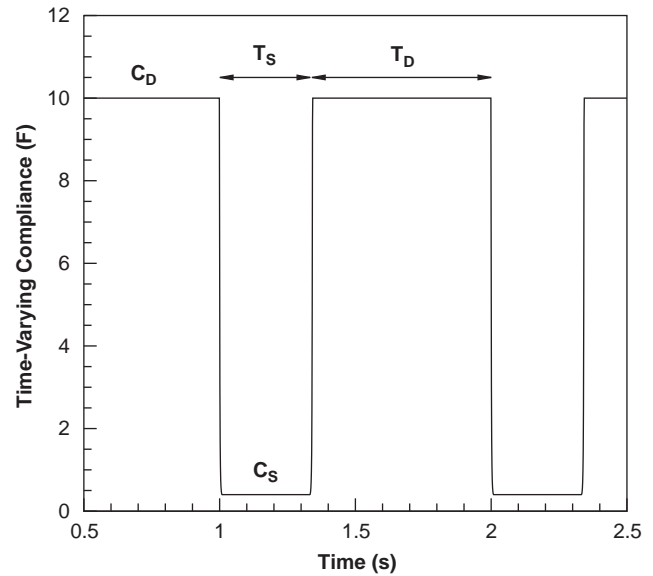

Fig. 2. Time-varying compliance waveform.

ratios are trivially accommodated. Voltages in this circuit analog represent pressures, and currents represent flows.

The arterial and venous compartments are characterized by constant resistances and compliances. The system is thus described by a set of three coupled time-invariant linear differential equations:

$$\frac{d}{dt}[C(t)V_0(t)] = [i_2(t) - i_0(t)],$$

$$\frac{d}{dt}V_1(t) = \frac{1}{C_1}[i_0(t) - i_1(t)],$$

$$\frac{d}{dt}V_2(t) = \frac{1}{C_2}[i_1(t) - i_2(t)]. \tag{1}$$

The currents can be expressed using the constitutive relations for the resistors:

$$i_0(t) = \frac{1}{R_0}[V_0(t) - V_1(t)],$$

Table 1
Parameter assignments and initial conditions for the pulsatile model

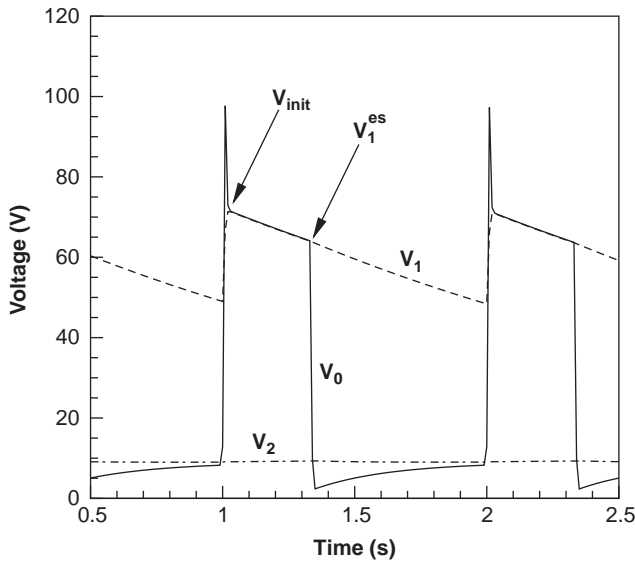|	Compartment		
	0	1	2
R (Ω)	0.01	1.0	0.03
C (F)	0.4–10.0	2.0	100.0
V_{initial} (V)	7.0	56.0	9.0

Fig. 3. Voltage waveforms generated using the pulsatile model. V_1^{es} and V_{init} are defined here for future reference.

$$i_1(t) = \frac{1}{R_1}[V_1(t) - V_2(t)],$$

$$i_2(t) = \frac{1}{R_2}[V_2(t) - V_0(t)]. \tag{2}$$

Table 1 shows the parameter assignments and initial conditions for the pulsatile model (Davis & Mark, 1990).

Fig. 3 shows the voltage waveforms generated with the pulsatile model described above.

It should be pointed out that the spikes in the voltage V_0 are non-physiologic and not seen if a more realistic time-varying compliance waveform is used (see Appendix A, which also points to recent analytical solutions of the pulsatile model). Fig. 4 shows the transient response of the voltage waveforms to a step in the resistance R_1 at time $t = 5$ s and demonstrates that changes in the cycle-
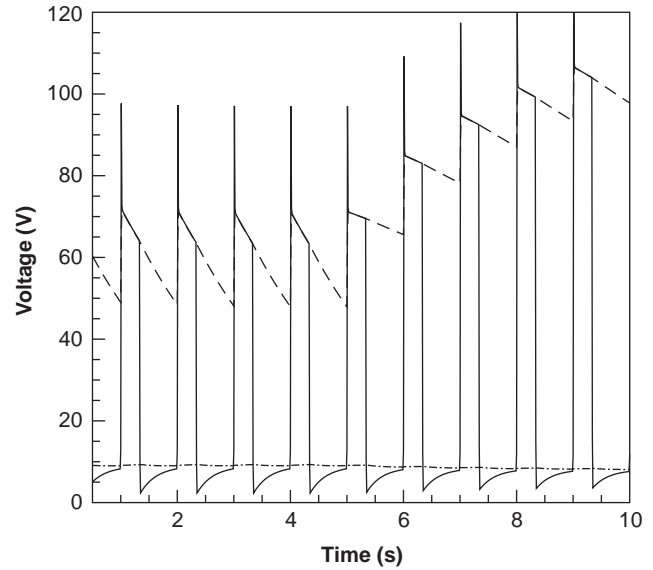

Fig. 4. Transient response of pulsatile waveforms to a step change in the resistance R_1 from 1.0 to 5.0 Ω at time $t = 5$ s.

to-cycle dynamics occur over time scales that are large compared to the time scale of intra-cycle dynamics.

3. Developing a cycle-averaged model

In developing a cycle-averaged version of the simplified cardiovascular model, we make use of the definition of the symmetric running (or local) time-average of a waveform $V(t)$ over a period T:

$$\langle V(t) \rangle = \frac{1}{T} \int_{t-T/2}^{t+T/2} V(\tau) \, d\tau. \tag{3}$$

If $V(t)$ is periodic with period T, then $\langle V(t) \rangle$ will evidently be constant, but departures from this periodicity result in time-varying $\langle V(t) \rangle$.

An important consequence of Eq. (3) is that the derivative of the time-averaged waveform equals the time-average of its derivative, i.e.

$$\left\langle \frac{d}{dt} V(t) \right\rangle = \frac{d}{dt} \langle V(t) \rangle. \tag{4}$$

When averaging constraint equations for terminal voltages, currents, and charges of linear and time-invariant components of the circuit, one can easily verify that the time-averaged voltages, currents, and charges obey the same constraints as their instantaneous counterparts. Our attention in finding a cycle-averaged description of the pulsatile model therefore focuses on finding a cycle-averaged description of the elements that give rise to the nonlinear and time-varying nature of the circuit, namely the diodes and the time-varying elastance.

3.1. Replacing the time-varying elastance

The cycle-averaged voltage across the central capacitor is given by

$$\langle V_0(t) \rangle = \langle E(t)Q(t) \rangle, \tag{5}$$

where $Q(t)$ is the instantaneous charge on this capacitor. If $Q(t)$ were of low ripple,[1] one could approximate the average of the product on the right-hand side by the product of the averages. In the pulsatile model described above, however, $Q(t)$ has a relative peak-to-peak ripple of approximately 100%, which is certainly not low ripple. We therefore expand both $E(t)$ and $Q(t)$ in Fourier series to first order:

$$E(t) \approx E_0 + E_1 \cos\left(\frac{2\pi t}{T}\right) + E_2 \sin\left(\frac{2\pi t}{T}\right),$$

$$Q(t) \approx Q_0 + Q_1 \cos\left(\frac{2\pi t}{T}\right) + Q_2 \sin\left(\frac{2\pi t}{T}\right). \tag{6}$$

The right-hand side of Eq. (5) can now be approximated by

$$\langle E(t)Q(t) \rangle \approx E_0 Q_0 + \tfrac{1}{2}(E_1 Q_1 + E_2 Q_2), \tag{7}$$

where E_0 and Q_0 are equivalent to $\langle E(t) \rangle$ and $\langle Q(t) \rangle$, respectively. Since, for now, $E(t)$ is strictly periodic, E_0, E_1, and E_2 are constant. Furthermore, Q_1 and Q_2 can be assumed constant over the cycle period T. The second term on the right-hand side of Eq. (7) therefore represents an offset voltage, V_{offset}, that is approximately constant over the averaging interval. Eq. (5) therefore equates to

$$\langle V_0(t) \rangle \approx \langle E(t) \rangle \langle Q(t) \rangle + V_{\text{offset}}. \tag{8}$$

The time-averaged rate of change of the charge on the central capacitor, i.e. the current flowing into or out of the capacitor, can now be evaluated using Eq. (8):

$$\langle i(t) \rangle = \frac{d}{dt}\langle Q(t) \rangle \approx \frac{d}{dt}\left(\frac{\langle V_0(t) \rangle - V_{\text{offset}}}{\langle E(t) \rangle}\right)$$

$$= \frac{1}{\langle E(t) \rangle}\frac{d}{dt}\langle V_0(t) \rangle. \tag{9}$$

The final equality in Eq. (9) follows from the constancy of $\langle E(t) \rangle$ and V_{offset}, respectively. Using the definitions in Fig. 2, $\langle E(t) \rangle$ is given by

$$\langle E(t) \rangle = \frac{T_S}{T C_S} + \frac{T_D}{T C_D}. \tag{10}$$

The time-varying elastance introduced in Section 2 can therefore be replaced by a constant capacitor with effective capacitance $C_{\text{eff}} = 1/\langle E(t) \rangle$ and constant offset voltage V_{offset} as indicated in Fig. 5.

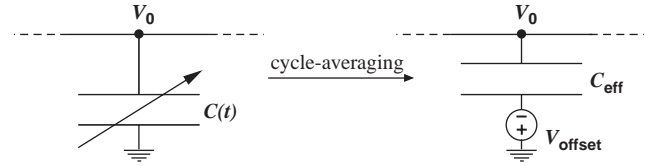[1]The relative peak-to-peak ripple of a waveform V is $V_{\text{pp}} = (V_{\max} - V_{\min})/\langle V \rangle$.

Fig. 5. Effect of averaging the time-varying capacitance.

3.2. Replacing the diodes D_1 and D_2

To deal with the diodes D_1 and D_2, we introduce a switching function $q(t)$ that is 1 when the diode D_1 is conducting and 0 when D_1 is non-conducting. The square-wave nature of the time-varying compliance waveform allows for two simplifications: (1) $q(t) = 1$ throughout T_D and $q(t) = 0$ throughout T_S; and (2) a switching function for D_2 is given by $[1 - q(t)]$, i.e. D_2 is conducting when D_1 is not and vice-versa. To study the currents through the diodes, it will be convenient to introduce the following voltages (also see Fig. 1):

$$V_{\text{out}}(t) = [1 - q(t)]V_0(t) + q(t)V_1(t),$$

$$V_{\text{in}}(t) = [1 - q(t)]V_2(t) + q(t)V_0(t). \tag{11}$$

The time averages of the currents i_0 and i_2 can now be represented using the switching function $q(t)$:

$$\langle i_0(t) \rangle = \frac{1}{R_0}(\langle V_{\text{out}}(t) \rangle - \langle V_1(t) \rangle)$$

$$= \frac{1}{R_0}(\langle V_0(t) \rangle - \langle q(t)V_0(t) \rangle)$$

$$+ \frac{1}{R_0}(\langle q(t)V_1(t) \rangle - \langle V_1(t) \rangle), \tag{12}$$

$$\langle i_2(t) \rangle = \frac{1}{R_2}(\langle V_2(t) \rangle - \langle V_{\text{in}}(t) \rangle)$$

$$= \frac{1}{R_2}(\langle q(t)V_2(t) \rangle - \langle q(t)V_0(t) \rangle). \tag{13}$$

The remainder of this sub-section will be devoted to finding appropriate approximations to the terms in Eqs. (12) and (13) that are averages of a product of the switching function with one of the voltage waveforms. We seek approximations invoking combinations of averaged waveforms to replace the averages of combinations of waveforms.

Diastolic venous waveform: $\langle q(t)V_2(t) \rangle$ represents the cycle-averaged diastolic venous waveform. Owing to the large value of C_2, V_2 is approximately constant around the value $\langle V_2(t) \rangle$, as can be seen from Fig. 3. It is therefore appropriate to approximate the diastolic venous waveform by

$$\langle q(t)V_2(t) \rangle \approx \langle q(t) \rangle \langle V_2(t) \rangle = \frac{T_D}{T}\langle V_2(t) \rangle. \tag{14}$$

Diastolic cardiac waveform: $q(t)V_0(t)$ represents the cardiac waveform during diastole, $V_0^d(t)$. Its time course can be expressed as follows:

$$V_0^d(t) = V_0^{bd} + (V_2(t) - V_0^{bd})(1 - e^{-t/C_D R_2}). \qquad (15)$$

By invoking continuity of charge, the cardiac voltage at the beginning of diastole, V_0^{bd}, can be expressed in terms of the arterial end-systolic voltage, V_1^{es}, according to

$$V_0^{bd} = \frac{C_S}{C_D} V_1^{es}. \qquad (16)$$

Inserting Eq. (16) into Eq. (15) and applying the cycle-averaging operation results in a cycle-averaged expression for the diastolic cardiac waveform

$$\langle q(t)V_0(t) \rangle = \frac{R_2}{T}(C_D \langle V_2(t) \rangle - C_S V_1^{es})(e^{-T_D/C_D R_2} - 1). \qquad (17)$$

Eq. (17) necessitates finding an expression for V_1^{es} in terms of the other cycle-averaged voltages.

End-systolic arterial voltage: To find an expression for the end-systolic arterial voltage, V_1^{es}, we make a straightline approximation of the arterial voltage waveform $V_1(t)$ with a slope of $-V_{init}/R_1 C_1$, as suggested by Fig. 3. Under this assumption, it can be easily verified that V_1^{es} is given by

$$V_1^{es} = \langle V_1(t) \rangle \frac{2R_1 C_1 - 2T_S}{2R_1 C_1 - T}. \qquad (18)$$

Diastolic arterial voltage: The diastolic portion of the arterial waveform can be approximated by

$$V_1^d(t) = (V_1^{es} - V_2(t)) e^{-t/R_1 C_1} + V_2(t), \qquad (19)$$

so that the cycle-averaged diastolic arterial waveform is given by

$$\langle q(t)V_1(t) \rangle = \frac{T_D}{T} \langle V_2(t) \rangle + \frac{R_1 C_1}{T}(V_1^{es} - \langle V_2(t) \rangle)$$
$$\times (1 - e^{T_D/R_1 C_1}) \qquad (20)$$

into which the right-hand side of Eq. (18) can be substituted.

3.3. Model structure and initial conditions

When combining the results of the last four subsections with Eqs. (1,9,12,13), it emerges that the resultant cycle-averaged model can be represented by the LTI circuit model in Fig. 6, where the diodes have been replaced by voltage and current sources that depend on the cycle-averaged voltages $\langle V_0(t) \rangle$, $\langle V_1(t) \rangle$, and $\langle V_2(t) \rangle$. Equivalently, the model is described by a state–space model of the form

$$\frac{d}{dt} \begin{bmatrix} \langle V_0(t) \rangle \\ \langle V_1(t) \rangle \\ \langle V_2(t) \rangle \end{bmatrix} = \begin{bmatrix} & A & \end{bmatrix} \begin{bmatrix} \langle V_0(t) \rangle \\ \langle V_1(t) \rangle \\ \langle V_2(t) \rangle \end{bmatrix}. \qquad (21)$$
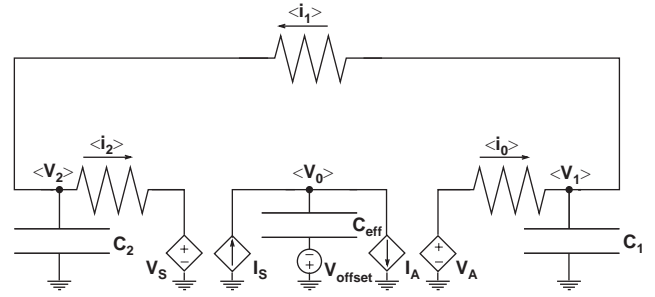

Fig. 6. Circuit representation of the cycle-averaged model. V_s, V_A, I_s, and I_A are controlled voltage and current sources that depend on the cycle-averaged voltages in the circuit.

An eigenvalue decomposition of A reveals the following eigenvalues $[\lambda_1, \lambda_2, \lambda_3] = [-109.02, -0.68, 0.0]$. The negative reciprocals of the three eigenvalues of A are the time constants of the exponentials that govern the response of the model to initial conditions. The eigenvalue λ_1 is irrelevant to our simulations as it corresponds to a time constant much smaller than our averaging interval T. The second eigenvalue corresponds to a time constant of approximately 1.49 s. The final eigenvalue, $\lambda_3 = 0$, with its corresponding eigenvector $E_3 = [E_{31}, E_{32}, E_{33}]'$, indicates that a non-zero steady-state solution exists. In fact, after initial transients due to λ_1 and λ_2 have subsided, the system will settle in a new steady-state S proportional to E_3

$$S = \gamma E_3, \qquad (22)$$

where γ is determined by the total charge in the system, according to the constraint

$$Q_{total} = [C_{eff}, C_1, C_2] \begin{bmatrix} \gamma E_{31} - V_{offset} \\ \gamma E_{32} \\ \gamma E_{33} \end{bmatrix}. \qquad (23)$$

We can determine γ by requiring that the total charge in the cycle-averaged model equal the total charge in the pulsatile model. The state S then becomes a natural choice for the initial conditions of the cycle-averaged model. Using the waveforms generated by the pulsatile model, the offset pressure can be computed to $V_{offset} = -14.5078$. The total charge of the pulsatile model is 1082C, which leads to $\gamma = 70.69$. Thus the initial condition for the cycle-averaged model is given by $S' = [27.8382, 64.3432, 9.0626]$.

4. Comparison of simulations

To evaluate the performance of the cycle-averaged model we will compare its simulation results and simulation time to that of the pulsatile model.

Table 2
Comparison of steady-state simulation results for the pulsatile model
(PM) and the cycle-averaged model (CAM)

Variable	PM	CAM	Rel. Error (%)
V_0 (V)	29.23	27.85	−4.7
V_1 (V)	64.07	64.36	0.5
V_2 (V)	9.01	9.06	0.6
i_0 (A)	55.06	55.30	0.4
i_1 (A)	55.06	55.30	0.4
i_2 (A)	55.09	55.30	0.4
q_0 (C)	53.03	47.06	−11.26
q_1 (C)	128.14	128.72	0.5
q_2 (C)	900.83	906.22	0.6

Values shown under PM are cycle-averages of the pulsatile waveforms.

4.1. Comparison of steady-state numerics

In Table 2, the steady-state responses of the cycle-averaged model (CAM) and cycle-averages in the pulsatile model (PM) are compared. All but two of the steady-state values show a negligible discrepancy between the cycle-averaged and the pulsatile model. The remaining two variables are not independent, and an improvement in V_0 will certainly led to an improvement in q_0. One could tune the offset voltage V_{offset} in the cycle-averaged model to reduce the discrepancy of V_0 between the cycle-averaged and the pulsatile model.

4.2. Comparison of dynamic responses

To compare the responses of the two models to changes in their parameters, we chose to perturb (1) the resistance R_1, and (2) the cycle period T. Both parameters play important roles in cardiovascular homeostasis through feedback regulation, and both have the capacity to change by a factor of 2 over short periods of time. Fig. 7 shows the beat-by-beat cycle-averaged response of the pulsatile model (solid line) and the response of the cycle-averaged model (dashed line) to a change in R_1. At time $t = 15\,\text{s}$, the resistance is ramped from $R_1 = 1.0$ to $2.0\,\Omega$ over a period of 2 s. At time $t = 45\,\text{s}$, this process is reversed.

Fig. 8 shows the transient dynamics of both models when the cycle period is changed in a step from $T = 1.0 - 0.5\,\text{s}$. The step is again reversed at $t = 45\,\text{s}$. Both transient simulations show that the time constants of the system-level response are preserved well by the cycle-averaged model. The main discrepancy between the simulation outputs of the two models is the static offset in the steady-state value of V_0.

4.3. Computational efficiency

Both the pulsatile and the cycle-averaged models were implemented in the C programming language using a
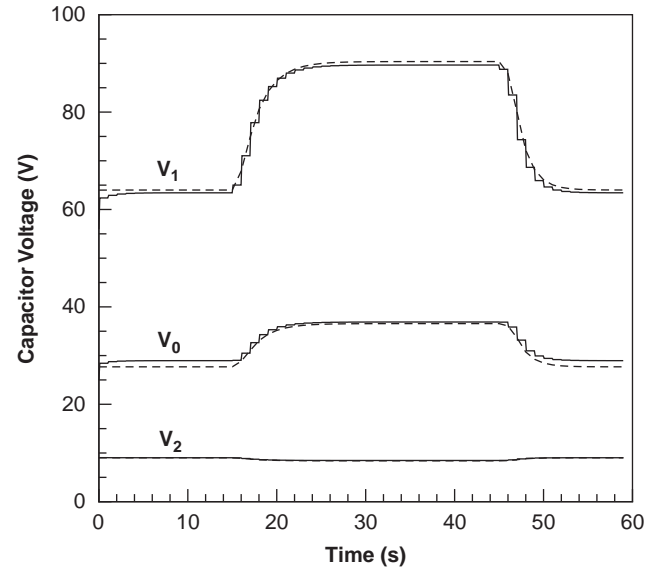

Fig. 7. Transient response to changes in R_1. CAM: dashed line; PM: solid line, showing beat-by-beat cycle-averaged waveforms.
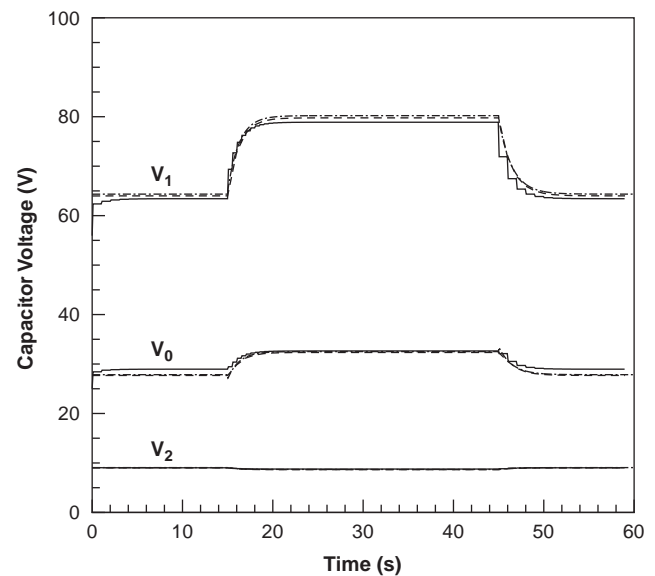

Fig. 8. Transient responses to changes in T. CAM: dashed lines; PM: solid lines, showing beat-by-beat cycle-averaged waveforms.

Linux operating system on a PC (AMD Athlon XP 2000+, 1.67 GHz processor). A standard fourth-order Runge–Kutta integrator was used to solve the differential equations numerically. In order to compare computational efficiencies between the various models, we make use of the fact that total charge is a conserved quantity in both implementations. The step-sizes were chosen in such a way that a pre-defined, relative numerical error in total charge was not exceeded throughout the numerical integrations. In Table 3, we present the steady-state voltages of the pulsatile model and of the cycle-averaged model for three different step

Table 3
Computational efficiency vs. simulation accuracy

Variable	PM		CAM	
Step size (s)	10^{-6}	10^{-4}	10^{-3}	10^{-2}
V_0 (V)	29.23	27.85	27.85	27.85
V_1 (V)	64.07	64.36	64.36	64.36
V_2 (V)	9.01	9.06	9.06	9.06
CPU time (s)	10083.9 ± 88.2	121.3 ± 0.5	12.3 ± 0.2	1.2 ± 0.1

Table 4
Comparison of pulsatile, cycle-averaged, and reduced-order model

Variable	PM	CAM	ROM
Step size (s)	10^{-6}	10^{-2}	10^{-1}
V_0 (V)	29.23	27.85	27.85
V_1 (V)	64.07	64.36	64.36
V_2 (V)	9.01	9.06	9.06
CPU time (s)	10083.9 ± 88.2	1.21 ± 0.04	0.11 ± 0.01

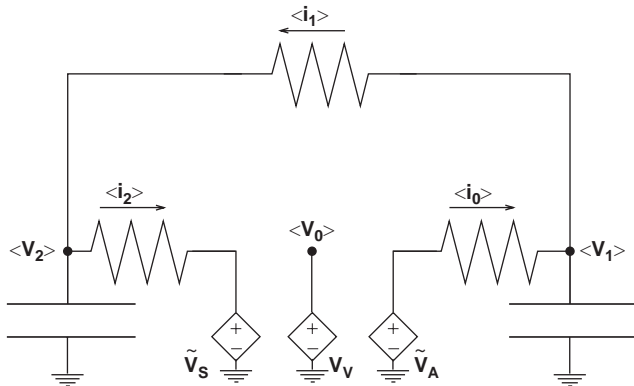CPU times show mean $\pm$ standard deviation.

Fig. 9. Circuit representation of the reduced order model. V_V, $\tilde{V}_S$, and $\tilde{V}_A$ are controlled voltage sources that depend on the cycle-averaged voltages $\langle V_1(t) \rangle$ and $\langle V_2(t) \rangle$.

sizes. The source codes were compiled using the -pg option of the gcc compiler. Each program was run for 10,000 s of simulated time and Linux's Gprof utility was used to assess the CPU time. In each run, the simulation shown in Fig. 7 is repeated with a period of 100 s. The final steady-state values at the conclusion of the simulations are reported in Table 3; the CPU times given in the table are averages of five separate runs for each program.

As can be seen from this table, the CPU time for the cycle-averaged model can be improved by a factor of 8000 over the pulsatile model without serious degradation of accuracy.

The estimate of computational cost of the pulsatile model might be somewhat exaggerated due to the choice of ventricular pressure as a state variable. Choosing ventricular volume instead might allow for bigger time steps to be taken, while conserving simulation accuracy, such that the pulsatile model does not perform so unfavorably. Nevertheless, the averaged model clearly permits substantial efficiencies over the pulsatile model.

5. Model reduction

As noted in Section 3.3, the cycle-averaged model has one very fast time constant $\tau_1 = -1/\lambda_1 \approx 0.009$ s. As mentioned before, this time constant is much smaller

than our averaging interval and is therefore irrelevant to the cycle-averaged model. Using ideas from singular perturbation theory (see, e.g., Caliskan, Verghese, & Stanković, 1999), we can accordingly partition the cycle-averaged state-space model as follows:

$$\begin{bmatrix} \dot{x}_f \\ \dot{x}_s \end{bmatrix} = \begin{bmatrix} A_1 & A_2 \\ A_3 & A_4 \end{bmatrix} \begin{bmatrix} x_f \\ x_s \end{bmatrix}, \tag{24}$$

where x_f and x_s correspond to rapidly and slowly varying signals, respectively. In our case, the structure of the matrix A in Eq. (21), suggests that x_f corresponds to $\langle V_0 \rangle$ and x_s to $[\langle V_1 \rangle, \langle V_2 \rangle]$. Since x_f is a signal with a very fast transient, $\dot{x}_f$ will be approximately zero after a short-time interval. Consequently, x_s can be written as follows in terms of x_f following the fast transient interval:

$$x_f \approx -A_1^{-1} A_2 x_s. \tag{25}$$

Substituting this in the expression for $\dot{x}_s$ yields a reduced-order cycle-averaged model, still in state-space form

$$\dot{x}_s \approx (A_4 - A_3 A_1^{-1} A_2) x_s. \tag{26}$$

The circuit representation of the reduced order model (ROM) is shown in Fig. 9.

In Table 4, we compare the steady-state capacitor voltages and CPU times for the largest possible time steps that the pulsatile, the cycle-averaged, and the reduced-order models permit. The CPU times are again based on 10,000 s simulations, and represent the averages of five separate runs of each program.

In Fig. 10, we compare the dynamic response of the three models to a ramp in the resistance R_1 from 1.0 to 2.0 Ω at $t = 15$ s.

Note that the reduced-order CAM runs 10 times faster than the CAM. The only noticeable difference in the dynamic responses is seen in the arterial voltage V_1 after the new steady state is attained. The relative error in V_1 between the ROM and the PM responses is only 2.3%, however, and therefore well within the tolerable range for the approximations made.
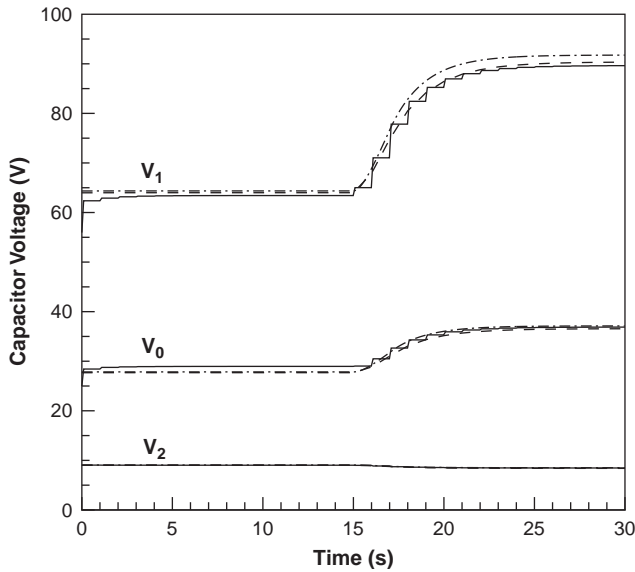
Fig. 10. Ramp in resistance R_1 at time $t = 15$ s. PM: solid line; CAM: dashed line; ROM: dash-dotted line.

6. Conclusions

In this paper, we have applied circuit-averaging techniques to a simplified lumped-parameter model of the cardiovascular system. We have shown that the resultant model structure is linear and time invariant, which allows for further insight into the model structure as demonstrated by our analysis of eigenvalues and eigenvectors. The realization of a fast time-constant also leads to the development of a reduced-order model using singular perturbation techniques. The cycle-averaged models allow for more generous time steps, which reduces the CPU time by a factor of 8000 for the full CAM and 80,000 for the reduced CAM, while still preserving accuracy of the simulation output. It has to be pointed out, however, that the small time step required by the PM is due to a somewhat conservative restriction placed on the relative error of total charge; relaxing this restriction or choosing volume instead of pressure as state variable will allow somewhat bigger time steps.

It is our main conclusion that cycle-averaging is a powerful technique to single out cardiovascular dynamics that occur on the time scale of a few cycles. Improvements in computational efficiency and insight into the model structure are gained by focusing on those components of the model that give rise to the dynamics of interest. Future work will include an improvement in the representation of $V_0(t)$, choice of ventricular volume as a state variable, more realistic compliance variation, extension to multi-chamber heart models, and addition of cardiovascular reflex mechanisms to allow for homeostatic control.

Appendix

Assuming a piecewise linear time-varying elastance waveform (see Fig. A1), Chen (Chen, 2003a; Chen, Heldt, Verghese, & Mark, 2003b) obtained more realistic voltage waveforms as shown in Fig. A2. In fact, by making reasonable approximations, analytical solutions (top panel of Fig. A2) can be obtained that compare very favorably to the numerical ones (bottom panel of Fig. A2), both in terms of the steady-state numerics and the transient response to perturbations of parameters. In Fig. A2, for example, the cycle-period T
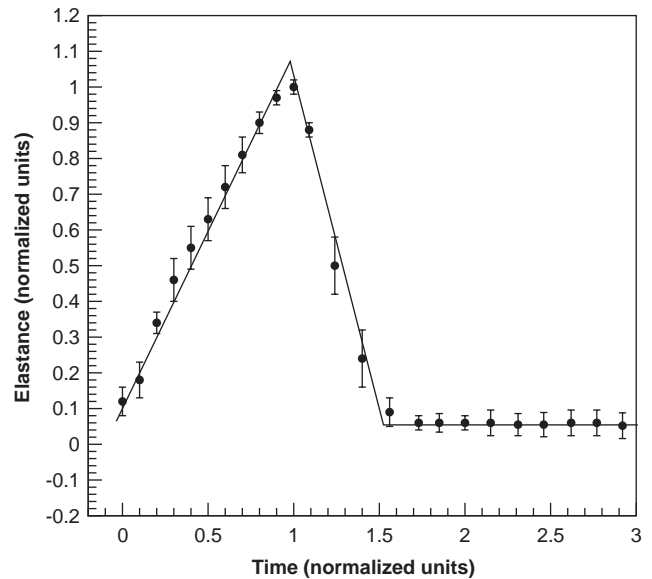

Fig. A1. Piecewise linear time-varying elastance waveform. Data adapted from (Senzaki, Chen, & Kass, 1996).
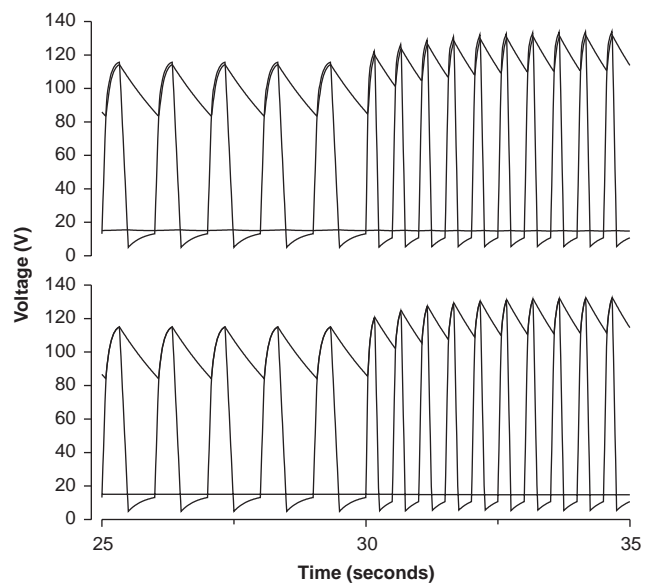

Fig. A2. Voltage waveforms generated using a more realistic time-varying elastance profile.

is halved at time $t = 30\,\text{s}$. While in principle cycle-averaging can be applied to the piecewise linear elastance model of Fig. A1, increased computational efficiency was achieved in this case by sampled-data methods rather than local averaging. We are currently exploring averaging for this elastance model.

References

Caliskan, V. A., Verghese, G. C., & Stanković, A. M. (1999). Multifrequency averaging of DC/DC converters. *IEEE Transactions on Power Electronics*, *14*(1), 124–133.

Chang, J. L. (2002). *Cycle-averaged models of cardiovascular dynamics*. M. Eng. thesis, Department of Electrical Engineering and Computer Science, Massachusetts Institute of Technology.

Chen, J. J. S. (2003a). *Analytical solution to a simplified circulatory model using piecewise linear elastance function*. M.S. thesis, Department of Electrical Engineering and Computer Science, Massachusetts Institute of Technology.

Chen, J. J. S., Heldt, T., Verghese, G. C., & Mark, R. G. (2003b). Analytical solution to simplified circulatory model using piecewise linear elastance function. *Computers in Cardiology*, *30*, 259–262.

Davis, T. L., & Mark, R. G. (1990). Teaching physiology through simulation of hemodynamics. *Computers in Cardiology*, *17*, 649–652.

Heldt, T., Shim, E. B., Kamm, R. D., & Mark, R. G. (2002). Computational modeling of cardiovascular response to orthostatic stress. *Journal of Applied Physiology*, *92*, 1239–1254.

Senzaki, H., Chen, C. H., & Kass, D. A. (1996). Single-beat estimation of end-systolic pressure–volume relation in humans. *Circulation*, *94*, 2497–2506.

Sunagawa, K., & Sagawa, K. (1982). Models of ventricular contraction based on time-varying elastance. *Critical Reviews in Biomedical Engineering*, *7*(3), 193–228.

Verghese, C. G. (1996). Dynamic modeling and control in power electronics. In: W. S. Levine (Ed.), *The control handbook* (pp. 1413–1424). Boca Raton: IEEE Press.